Maritime RobotX journal paper

Flinders University / Australian Maritime College – Team Topcat

Flinders University team members

Assoc. Professor Karl Sammut, Jonathan Wheare, Dr. Andrew Lammas, Mr Richard Bowyer, Matthew Anderson, Thomas Arbon, Bradley Donnelly, Russell Peake, Tenzin Crouch, Rowan Pivetta, Joshua Renfrey, Tobias Wooldridge, Scott Stevens, Andrew Webb.

Australian Maritime College team members

Dr. Alexander Forrest, James Keane, Harry Hubbert, Reuben Kent, Supun Randeni

1.Abstract

Fifteen teams from five countries will be converging on Singapore for the 2014 Maritime RobotX challenge. This competition requires the construction of an autonomous electric boat based on a standardised hull.

A range of competitive tasks have been specified by the challenge organisers requiring techniques in areas as diverse as maritime engineering, software development, image processing, sonar localisation and vehicle guidance. This document describes the technical approach taken by Team Topcat - a collaboration between Flinders University and the Australian Maritime College to build a vessel for the competition. Details include the vessel design, sensor processing, classification systems, guidance and control of the vehicle.

2.Introduction

This journal paper outlines the autonomous surface vehicle (ASV) developed by the combined Flinders University / Australian Maritime College (AMC) team for the 2014 Maritime RobotX Challenge [1].

For this competition, teams were provided with a standardised platform developed by Marine Advanced Research in their Wave Adaptive Multipurpose Vessel (WAM-V)[2] series. Teams have been required to adapt this vessel for autonomous operation by the addition of engines, sensors and computer equipment allowing them to complete the tasks specified by the competition rules.

The Flinders University – Australian Maritime College (AMC) team proved a good combination. AMC is renown for its naval architecture programs and has world-class hydrodynamic test facilities. Flinders University has expertise in robotics and has competed in other robotics competitions. Work was broken down such that AMC was responsible for the design and fabrication of the engine pods and determining the vehicle's hydrodynamics, while Flinders University concentrated on the electrical systems, sensors, software and autonomy. Although the geographical distance between the Flinders (based in South Australia) and AMC (based in Tasmania) groups was challenging, the two groups worked very well together. The WAM-V was initially shipped in February to AMC and then transferred to Flinders at the end of June.

This document will outline the approach taken by our team in the construction of the vehicle and our current results.

3.Technical Approach

Our objectives in the development of the vessel include not only applicability for the competition, but also to produce a system that can be applied as a research and monitoring platform after the competition. Our vessel has thus been designed to maximise its range, payload capacity and the field of view of its sensors while maintaining a low centre of gravity.

On an electric vehicle, power must be provided for both the motive systems and the computing and sensor systems (hotel load). For a long duration system, the batteries contribute a significant proportion of the vehicle mass. Mounting the battery on the payload tray would result in a system with a high centre of gravity and a corresponding potential decrease in stability. Our design lowers the height of the centre of gravity by splitting the primary battery into two halves, each mounted in the waterproof compartment of the two engine pods.

To provide the required autonomy, we have developed software using the Robotics Operating System (ROS) [3]. The modularity of ROS has allowed independent development of programs ("ROS nodes") as well as allowing the use of third party packages.

3.1. Platform

3.1.1. Propulsion

Various propulsion units were considered. A pair of Torqeedo Cruise 2R electric outboard motors were eventually selected due to their performance (520N static thrust and 1120W power at 56% efficiency) and their proven compatibility with the WAM-V platform. The motors can be driven independently to allow control of the vehicle heading by differential thrust. In our design, the thrust angle of the motors can also be changed independently within a range of +/- 30 degrees using a customised steering cable arrangement driven independently by a pair of Thomson Max Jac linear actuators mounted on the payload tray. This arrangement allows tighter steering and redundancy in the event of one thruster failing.

3.1.2. Hull design and hydrodynamics

The engine pods were designed by the AMC group to maximise the internal volume for battery storage while maintaining a ratio of 2:1 between the length and beam of the vessel [4].

The pods were fabricated from welded 5061 aluminium with the provided WAM-V adaptor bracket bolted to the front [4] – see Figure 1.

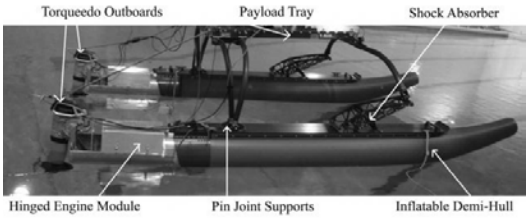

Figure 1 - Wave adaptable modular vessel with custom hinged engine modules.

At Flinders, the pods were further developed to accommodate the selected Lithium Polymer battery units and the battery management systems.

Once built the assembled vehicle was tested by AMC to collect quantitative hydrodynamic data, as well as observe the performance of the vessel to give the Flinders control team qualitative insight into the vessel behaviour's. The vessel

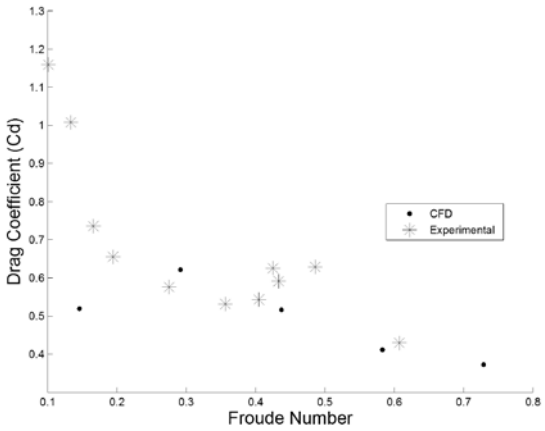

Figure 2 - Comparison of experimental and computational drag coefficients

hydrodynamics were determined through a bollard pull test to determine static propulsive thrust, and dynamic drag coefficients were determined through full-scale experiments and then validated

through Computational Fluid Dynamics (CFD) – see Figure 2. Hydrodynamic sway and yaw coefficients were determined, using semi-empirical formula and theoretical approaches.

Open water testing focused on vessel performance to derive the relationships between power and speed, between speed and the associated Froude number, and to gather qualitative insight into vessel manoeuvring abilities.

3.1.3. Superstructure design

The vehicle's superstructure design incorporates the mountings and housings for the vehicle's sensors, computing and electronic components. These components are required to be robust, waterproof and compatible with the WAM-V's ability to be rapidly assembled and disassembled.

The sensor mounts are comprised of two major components, the hydrophone deployment system and the platform mountings. The mechanical designs for these were modelled in Autodesk Inventor. The use of this CAD tool allowed a continual revision process with minimal overhead.

The biggest challenge in the mechanical design was to create the hydrophone deployment system. The WAM-V platform is designed with a payload tray that provides a relatively stable reference point, approximately one meter above the waterline. The pontoons are closer to the water but due to their independent ball joints provide a changing reference point complicating the development of the pinger location algorithms. To minimise the potential for localisation errors and to reduce unnecessary hydrodynamic drag from the hydrophone array, a retractable mounting that is rigidly attached to the payload tray was selected. Furthermore, the system was required to be robust and capable of carrying loads of up to 10kg to accommodate planned future research activities, extending to 1500mm and collapsing to approximately 500mm in order to ensure that sensors could both be safely retracted and effective when deployed.

A large variety of options for the deployment system were considered and evaluated on criteria including cost, capacity, strength, and manufacture time. The selected design was a telescope arm driven by a winch assembly powered through a worm drive reduction gearbox. To allow the required travel, the telescope is composed of four sections, each

500mm long with a 150mm (30%) overlap providing a good balance between quantity of sections and stability. The size of the tubes was selected to reduce manufacture time and cost, with prefabricated aluminium section used in all cases except for the outer tube, which was fabricated from four pieces of angle extrusion to reduce material costs. Acetal plastic runners were placed between tubes to ensure smooth movement. Finally, the outer section was stabilised with tension cables to minimize flex while moving.

The relative complexity of the upper mounting system was much lower than the sonar deployment system. The design was created to house all the sensors required (camera, LIDAR, RADAR, computer case and GPS) while minimising modifications to the WAM-V structure and ensuring sensors did not interfere or occlude each other.

3.1.4. Electrical design

The main battery system comprises a pair of Kokam Lithium Polymer (LiPo) batteries each rated at 25.8V nominal, 150 Ah and 3.8 kWh. Each of these batteries is mounted in an engine pod and paired with a battery management system (BMS) that monitors and balances the cell voltages.

To allow the hotel load to draw evenly from the battery modules, the paired supplies to the payload tray are connected to a diode network that draws from the battery with the highest voltage. This allows either module or a standby external supply to power the on-board systems. A small centrally located lead acid battery pack provides power to the BMS until main power is available.

Power regulation is provided by a quartet of non-isolated TI buck converters. Four voltage rails are produced at 5, 12, 19 and 22 Volts. Each rail provides a maximum of six amps. The power budget for the hotel load is eight Amps, but typical current draw is less than two.

3.1.5. Electronics enclosure

To ensure the safety of the delicate electronic equipment such as the power electronics and main computer boards, protection from the elements such as spray and rain must be provided. This must be balanced with the ability to reject waste heat from these components.

For our WAM-V we have selected a waterproof plastic case to enclose the power electronic and computing modules.

IP68 rated sockets and connectors are used to interface with external equipment and sensors, while heat is rejected using a water block mounted on an aluminium cold plate and connected to an external radiator.

3.1.6. Control

The choice of control inputs for the motors and actuators is derived from the commanded velocity targets using the vectorial model of rigid body dynamics applied to marine craft [5]. A high-level ROS C++ implementation was developed to produce the required control forces to be applied to the vessel in order to achieve a given input velocity command. This model can be presented as follows.

$$M\dot{v} + C(v)v + D(v)v = \tau$$

where:

v : Velocity state vector

$\dot{v}$: Acceleration vector

M: Inertia matrix (including added mass due to deflection of surrounding fluid)

$C(v)$: Coriolis and centripetal matrix (including added mass)

$D(v)$: Damping matrix (linear and non-linear drag terms)

τ: Vector of forces and moments applied to the vessel (control inputs)

Since the WAM-V is a surface vessel, a 3 degrees of freedom (DoF) model is sufficient to describe the controllable motion of the vessel. In 3-DoF only the surge (u), sway (v) and yaw rate (r) components of the vessel motion are considered. Figure 3 depicts the body frame and North-East-Down inertial frame of a 3-DoF ocean vessel.

In 3-DoF the parameters of the rigid body model are populated as follows:

$$M = M_{RB} + M_A =$$
$$\begin{bmatrix} m - X_{\dot{u}} & -X_{\dot{v}} & my_g - X_{\dot{r}} \\ -Y_{\dot{u}} & m - Y_{\dot{v}} & mx_g - Y_{\dot{r}} \\ my_g - N_{\dot{u}} & mx_g - N_{\dot{v}} & I_z - N_{\dot{r}} \end{bmatrix}$$

$$C(v) = C_{RB}(v) + C_A(v) =$$
$$\begin{bmatrix} 0 & 0 & -m(x_g r + v) \\ 0 & 0 & -m(y_g r - u) \\ m(x_g r - v) & m(y_g r - u) & 0 \end{bmatrix} +$$
$$\begin{bmatrix} 0 & 0 & -(Y_{\dot{v}} v + \frac{Y_{\dot{r}} + N_{\dot{v}}}{2} r) \\ 0 & 0 & X_{\dot{u}} u \\ Y_{\dot{v}} v + \frac{Y_{\dot{r}} + N_{\dot{v}}}{2} r & -X_{\dot{u}} u & 0 \end{bmatrix}$$

$$D(v) = D_L + D_{NL}(v) =$$

$$-\begin{bmatrix} X_u & 0 & 0 \\ 0 & Y_v & Y_r \\ 0 & N_v & N_r \end{bmatrix} -$$

$$\begin{bmatrix} X_{u|u|}|u| & 0 & 0 \\ 0 & Y_{v|v|}|v| + Y_{|r|v}|r| & Y_{|v|r}|v| + Y_{r|r|}|r| \\ 0 & N_{v|v|}|v| + N_{|r|v}|r| & N_r|v| + N_{|r|r}|r| \end{bmatrix}$$

$$v = \begin{bmatrix} u \\ v \\ r \end{bmatrix}, \qquad \tau = \begin{bmatrix} X \\ Y \\ N \end{bmatrix}$$

The entries in the matrices represent the vessel's mass (m), offset of the chosen body reference frame origin to the centre of mass (x_g, y_g), and the hydrodynamic characteristics which were determined by the team members from AMC.

The system model presented in the preceding section was implemented as a ROS node written in C++ utilising the uBLAS Boost [6] library for linear algebra operations. The target velocity command input is taken from a ROS topic which both the mission planning and tele-operation systems can publish data to, while the current state of the vessel is received from the localisation system and used to compute the required acceleration. The commanded velocity and required acceleration are then applied to the system model and used to derive the required control forces.

Using the control forces as determined by applying the velocity command and required acceleration to the system model, the control inputs are derived using geometric properties of the thruster configuration for differential thrust control allocation [7], and a pseudo-inverse approach for steered thruster (azimuth) control allocation. For the azimuth control allocation, the control inputs are determined using the following

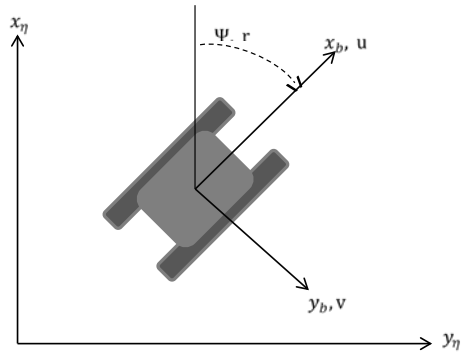

Figure 3 - Coordinate Reference Frames - 3 DOF Surface Vessel Model

equation [5]

$$\tau = TKu$$

where τ is the required control forces for a given velocity command, T is the thruster configuration matrix, K is a diagonal matrix of force coefficients and u is the control input vector. The control inputs are then determined by

$$u = K^{-1}T^{-1}\tau$$

Since T is generally a non-square matrix, the Moore–Penrose pseudo inverse is used to perform the inverse operation of the thruster configuration matrix.

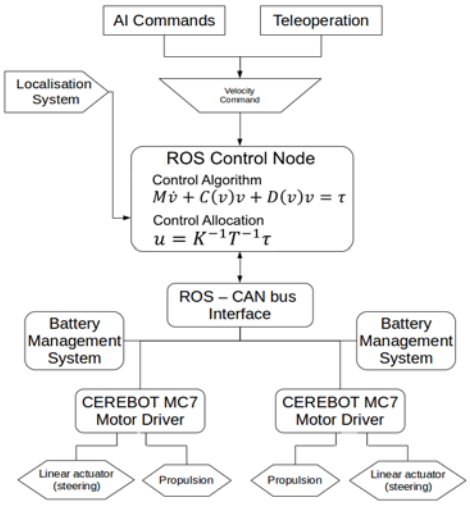

Figure 4 - WAMV Control Allocation System Block Diagram

After determining the control inputs required to drive the vessel to a given velocity state, these control inputs are published on a ROS topic. These commands are then processed by the ROS CAN node (an Arduino with a CAN shield) and transmitted to the motor control boards using the CAN bus.

A pair of Digilent Cerebot MC7 motor control boards receive the CAN messages generated by the high-level node. These controllers communicate with the Torqeedo motors, control the position of the linear actuators, and additionally control the motor that drives the sonar deployment system. Each board is independently powered by a Linear Technologies 24V voltage regulator board.

3.2. Sensors

For a robotic vessel to operate in a changing environment, it must have a method of perceiving its changing environment. The vehicle's sensors allow this perception to occur.

For our vessel, we have incorporated sensors capable of perceiving the outside world (camera, LIDAR, RADAR, Proximity) and tracking the motion of the vehicle itself (Global Positioning System (GPS) receiver, Attitude Heading Reference System (AHRS)). This section will outline the usage of these sensors on the vessel.

3.2.1. Computer Vision

The computer vision tasks required for three of the main challenges outlined in the competition guidelines comprise buoy detection, shape detection and colour sequence identification. The camera used is a Basler Ace acA1300-60gc with a wide-angle Theia rectilinear lens. Although, the lens causes some image distortion towards the corners of the image, it lacks the barrel distortion typically seen in fish-eye lenses. This wide angle lens gives the robot a 120^{o} field of vision which is useful

to allow it adequate coverage of obstacles and markers ahead of the robot.

The first vision task is the identification of red and green buoys for lane navigation. The input images are first converted from RGB (Red, Green, Blue) colour space to HSV (Hue, Saturation, Value) colour space. HSV colour space is more appropriate for colour filtering as it separates the hue component of each pixel from its intensity, which results in less sensitivity to changes in lighting conditions. Pre-processing is performed to reduce image artefacts and noise. This includes a Gaussian blur and image normalisation to ensure that the image has the maximum amount of contrast. Colour thresholding is then performed to set all pixels in an image with values above a threshold to "1" (white) and all others to "0" (black). This threshold was set empirically based on analysis of test images. Once a binary image has been produced with possible buoy locations, it is post-processed using morphological operations such as opening and closing, as well as analysing the shape of each blob. These operations ensure whether the detected object approximately matches the profile of the buoys on the course, thus helping to eliminate noise and false positives.

The second vision task involves the identification of the coloured light sequence on the light buoy. In a similar manner to the buoy detection algorithm, this task is achieved using colour thresholding and pre-processing of the input image to reduce image artefacts and noise.

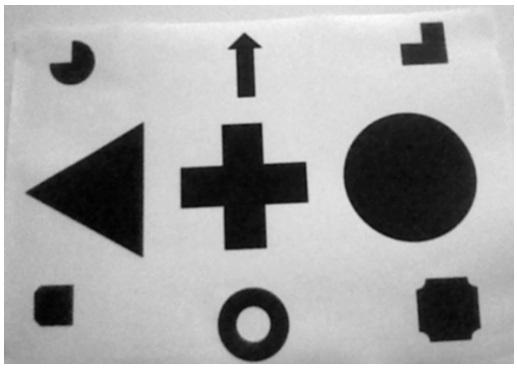

Figure 5- Greyscale input image

The symbol detection task is the most complicated of the three tasks. The shape detection algorithm begins by converting the input image into grayscale and filtering and normalising it, as shown in Figure 5.

Two binary images are created from the input. The first is created by thresholding for the light pixels in the image. The algorithm then takes the "holes" (black areas enclosed by white areas) in this image and creates a new binary image where the holes are positive. This is a more stringent test than simply

thresholding for dark pixels and forms the first of the two binary images. Secondly, Canny[8] edge detection is performed on the grayscale images as shown in Figure 6. The edges that don't form closed shapes are then discarded and closed edges filled in to create the second binary image.

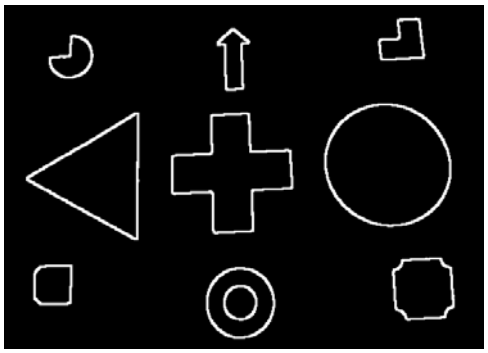

Figure 6 - Edge detection applied to greyscale image

A logical AND is performed on the two binary images to produce the final image that contains blobs for classification, as shown in Figure 7. Morphological opening and closing operations are performed on the image to eliminate noise and false positives.

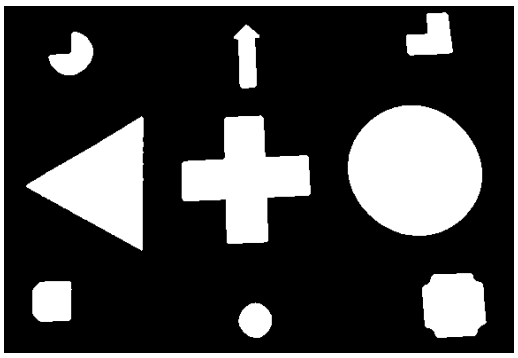

Figure 7 - combined image

For each white area (or "blob") in the above image, a bounding circle and convex hull are calculated. The bounding circle is the smallest circle that can be drawn to enclose the blob. The convex hull is the shortest curve that can be drawn around each blob. For example, the convex hull of a cross will have an octagonal shape. The bounding circle and convex hull can be used to classify the three types of shapes. The area of each blob is compared to the area of its bounding circle and convex hull. For a circle, these areas will be almost identical, with some disparity depending on the skew of the object to the camera. A cross will have a large disparity between the area of its bounding circle and convex hull, and its own area. A triangle will have a large disparity to the area of its bounding circle; however, the area of its convex hull will be almost identical. These conditions are used to determine a likely shape candidate for each blob.

For circles, this method does a good job of correctly identifying them without allowing through false positives. However to classify triangles and crosses, we need to confirm that they have the correct number of sides. An approximate curve is drawn around each blob. The approximation attempts to use the least line segments possible to encircle a blob without straying more than x pixels away from the original blob outline. The value of x is determined based on whether we believe the blob to belong to a cross or a triangle, and is based on the perimeter of the blob in question. The goal is to create the loosest approximation possible that will not alter the overall shape of the blob. After the approximation is created the number of sides is counted to determine its shape.

The result is shown in Figure 8. The algorithm does a good job of ensuring that no false positives are detected, while still tracking the docking symbols.

The computer vision algorithms were originally developed in Matlab and then written in C++ with the aid of the Open Source Computer Vision Library (OpenCV) to achieve real time performance [9].

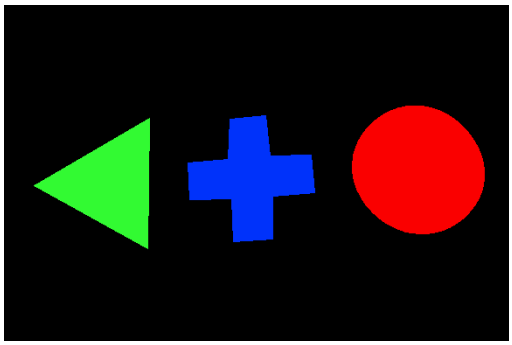

Figure 8 - result of shape detector

GPU Acceleration was tested on the shape detector algorithm, resulting in a 10% increase in frames processed per second. The speedup achieved is not significant as some functions in the program were not parallelisable, and consequently was not sufficient to warrant using GPU acceleration, although this decision will continue to be evaluated.

3.2.2. LIDAR

For obstacle detection and ranging, the vehicle uses a SICK LMS 511 LIDAR on a tilting mechanism. This subsystem was originally developed for the 2013 Autonomous Ground Vehicle Competition where it showed itself to be robust and reliable. LIDAR data is combined with the results of the image processing algorithms to identify the relative position of detected obstacles to the vehicle.

3.2.3. RADAR

To increase the perception range of the robot beyond the 80m available from the

SICK LIDAR, the WAM-V is equipped with a continuous wave Simrad 4G radar.

To allow the robot to use the data generated by the RADAR, we have developed a ROS driver based on a free-software plugin developed for the open source navigation maritime and tracking system OpenCPN. This driver produces a point cloud representation of the relative direction and intensity of the radar returns. This radar node allows it to seamlessly integrate into the navigation system.

We expect that the radar will be operating at a fraction of its 64km maximum range, where it will be used for search operations within the course. This range will allow the robot to be capable of detecting objects such as the floating dock or other vessels well before reaching the task elements. This capability allows mission planning for future areas of interest to be completed sooner, thus saving future time on the task at hand.

3.2.4. Pinger localisation

One of the competition tasks is to localise and report the location of a sonar pinger, which emits a repetitive pulse on a known frequency in the range of 25 – 40kHz. To perform this task, a 4 element hydrophone array (Teledyne Reson 4013) has been developed. The hydrophones are placed in an ultra-short baseline (USBL) array. This involves placing hydrophones in a known arrangement 150mm apart from each other and comparing the time of arrival of the signal at each hydrophone. The USBL approach is ideal as it's normal limiting factor – it's maximum range[10] – is avoided due to the search area being restricted to a rectangle approximately 40m wide and not more the 100m long.

To limit the amount of noise received by the digital signal processing system, the incoming signals are amplified and filtered by a custom amplifier board. This board contains four independent channels comprising operational amplifiers and programmable variable gain filters. This board has been designed to increase the signal to noise ratio by filtering out as much of the sound that is outside of the desired pinger frequency band. The amplifier then scales the incoming filtered signal into the voltage range expected by the 12-bit Analogue to Digital convertors on the host Digilent Nexys 4 Field Programmable Gate Array (FPGA) board which also serves to configure the amplifier board. The FPGA on the Nexys 4

board is used to process the digital signals. To obtain the Time Difference of Arrival (TDOA) information, the signals from the hydrophones are cross-correlated with each other. The max point of the cross-correlation will give the time difference between the signals.

By using the known geometric arrangement of the hydrophones and the TDOA, an estimate of the relative bearing of the sound source can be determined. By taking multiple readings at differing positions and compiling them in a fixed frame of reference relative to the DGPS supplied position of the robot, a solution for the location of the pinger can be identified.

3.2.5. Proximity

Proximity sensing aft of the robot is handled using a Leddar IS16 sensor. A ROS driver has been developed for this sensor as part of the project work. This sensor provides distance information to objects within a field of view of up to 45 degrees. This sensor will be most useful used for collision detection when the robot is reversing out of the dock.

3.2.6. Navigation state estimation

Tracking the position and velocity of the vessel is an important requirement in ensuring correct operation of both map building and vessel guidance. Our vessel uses a Trimble R10 differential GPS receiver for position and velocity and a Microstrain 3DM-GX3 AHRS to estimate heading and angular velocity. The output of these sensors is fused using a ROS package that implements an extended Kalman filter with a thirteen element state vector.

3.2.7. Safety and tele-operation

To minimise potential safety hazards, an emergency stop (e-stop) system has been developed that will cause the vessel to immediately halt the motion of its motors and linear actuators. This comprises two sections: one section comprises a wired e-stop that connects to three large switches, mounted along the rear supports and at the back end of the payload tray; and a remote wireless e-stop that is connected via radio to a hand-held unit. Either of these systems can cause the robot to halt.

The wireless e-stop consists of three parts: the main ESTOP controller on the WAM-V, running on an Arduino 2560 and connected to the host computer; a handset unit, running on an Arduino Leostick and supporting a USB game controller; and a Monitoring Station unit consisting of a Leostick connected to a

computer. All three units communicate via RFD900[11] modules running MultiPoint firmware using the MAVLINK[12] protocol with the unit on the WAMV acting as the central unit of the system. The ESTOP system has four distinct states: Linkloss, Stop, Manual and Auto. To ensure the system can retain control of the vehicle, messages are passed continually between the e-stop units and the vehicle. If there is no active communication then the Linkloss state is entered resulting in the vehicle halting.

In addition to Linkloss, the vehicle can be in three further states. Stop state halts the motors, but represents the e-stop as connected and ready. Manual state allows the e-stop to pass through joystick commands to the WAM-V's host computer for manual tele-operation of the vehicle, while Auto state disables these commands and instructs the host computer to begin autonomous operation. To be compliant with the RobotX rules regarding communication, in auto mode communication besides heartbeat and state transition messages are disabled. State transitions are controlled manually using red and green switches on the e-stop units.

To comply with Singapore's RF regulatory requirements the RFD 900 modules have been configured to use the frequency band of 920 – 925 MHz and the power output has been restricted to less than 200mW equivalent radiated power [13]. The bandwidth usage has been confirmed using a spectrum analyser.

The wired and wireless e-stops are wired to inputs on the Cerebot motor controllers. Both e-stop systems must be pulled high for the motors to function, with the Cerebot confirming the state of the e-stop before the transmission of each control packet.

3.3. Computing and Communication

The computing module for the vessel is required to have significant computing capabilities while maintaining the efficiency to both minimise power draw and the waste heat that requires rejection. To ensure compatibility with the ROS system, a Dell i7 laptop motherboard running Ubuntu Linux 12.04 was selected as the primary computing module. The bare motherboard is mounted on the cold plate within the computer box.

Communications with high speed sensors (LIDAR, RADAR, camera and hydrophones) is via a Gigabit Ethernet switch, while the

CAN bus, emergency stop state, LIDAR tilt, and proximity sensor communicate via Universal Serial Bus (USB).

During operation, a Wireless Access Point allows inspection of the vehicle's state. Since the vehicle can also be tele-operated through the e-stop system, this access point can be shut down during competition runs.

The control and autonomy system use the Hydro release of the Robotics Operating System (ROS) [3] as its underlying framework. ROS functions as a directional graph, with messages allowing communication between independent programs (ROS nodes). Development of autonomy components as independent programs with standardised interfaces allowed the individual sections to be developed largely independent of each other.

Use of a subsumption architecture for the highest level of the autonomy system was considered, but due to the requirement of attempting tasks in order, a simple python script that steps through each task in sequence will be used. The autonomy script dispatches commands to specialised subsystems via the actionlib system [14]. This allows goals to be passed and return status provided back to the host system.

Locations of interest are stored in latitude, longitude and clockwise heading from north. When operations require the calculation of distance and heading, the data is first converted into Universal Transverse Mercator and then the offset from a known datum point is calculated.

3.3.1. Simulation

To allow the development of autonomy and control software without risking the potential loss of vehicle that could result from real-world testing, an environment based on the Gazebo robotics simulator[15] has been developed. Developed for simulating the operation of field robots in three-dimensional environments, its ability to alter simulation behaviour with plugins has allowed the development of more varied platforms.

To simulate the WAM-V vehicle, a trio of gazebo plugins were developed;

- A hydrodynamic simulation of the WAM-V skis.
- A simulation of the Torqeedo motor.
- A controllable angle joint used for the Torqeedo mountings.

The ski and motor simulation plugins were based on hydrodynamic data derived from experimental and simulated data supplied by AMC.

The model has been populated with sensors including simulated LIDAR, cameras, AHRS and GPS. This allows the testing of sensor fusion and guidance in geodetic coordinates – see Figure 9.

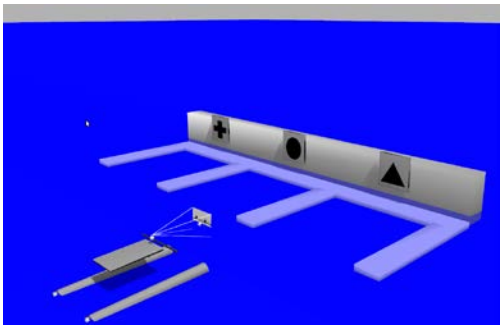

Figure 9 - Simulated WAM-V at shape recognition task.

3.4. Additional development

Upon assembly of the light buoy panel as specified by the technical directors, it was observed that a camera configured with a very short exposure for outdoor daytime use would have difficulties with the panel lighting scheme. At best only a few of the LED lines would be illuminated during the short exposure period. Investigation of the panel firmware showed that the LED scan rate could be greatly increased for the case where a solid block of colour is required.

A modified version of the firmware was developed and submitted to the RobotX directors who used it as the basis for an updated light buoy firmware.

4. Collaborations

Aside from the collaboration between the AMC and the Flinders University team members to build the robot, the team also collaborated with several equipment manufacturers to adapt the equipment to our requirements. We are indebted to Torqeedo GmbH for providing their communications software protocol, Kokam for constructing the LiPo battery to our requirements, and SICK for donating and assisting us with the LMS511 LIDAR.

5. Conclusion

This document has outlined the technical approach chosen by Team Topcat for the 2014 Maritime RobotX competition. We are looking forward to demonstrating our results in Singapore.

6. Acknowledgements

Team Topcat would like to thank the following staff and students, Mike Underhill, Jock Ferguson, Richard Stanley, Mark Walford, Craig Peacock, Darren Young, Tim Lilienthal, Dr. Irene Penesis, Dr. Jimmy Li, Dr. Sherry Randhawa, Dr.

Nasser Asgari, Isak Bowden-Floyd, Curtis Armstrong, Zac Pullen, Alex Waterhouse, Cameron Heron, Dave Carlsson, Jarrah Orphin, Sam Smith, Mitch Pearson, Dr. Rowan Frost, Zhi Leong, Konrad Zürcher and David Waldron, for their participation in the development of the vehicle. We are deeply indebted to our sponsors who generously provided their support by way of donated equipment/software and discounts: US Office of Naval Research, DSTO, Torqeedo Australia, SICK Australia, Teledyne Reson, LeddarTech, Motion Technologies, National Instruments, Mathworks, UPG Solutions, Aspitech, and Transmo Shipping.

7. Bibliography

[1] AUVSI Foundation, National University of Singapore School of Engineering, and Singapore Science Centre. (2014). *Maritime RobotX Challenge*. Available: http://www.robotx.org/

[2] Marine Advanced Reasearch Inc. . *Wave Adaptive Multipurpose Vessel*. Available: http://www.wam-v.com/index.html

[3] M. Quigley, B. Gerkeyy, K. Conleyy, J. Faust, T. Foote, J. Leibsz*, et al.*, "ROS: an open-source Robot Operating System," 2009.

[4] J. Keane, H. Hubbert, R. Kent, M. Haase, K. Sammut, J. Duffy*, et al.*, "Automating a Wave Adaptive Modular-Vessel as a Platform for Subsea Operations," 2014.

[5] T. I. Fossen, *Handbook of Marine Craft Hydrodynamics and Motion Control*: Wiley, 2011.

[6] J. Walter, M. Koch, G. Winkler, and D. Bellot. (2000-2011). *boost Basic Linear Algebra Library*. Available: http://www.boost.org/doc/libs/1_56_0/libs/numeric/ublas/doc/index.htm

[7] I. B. Wilhelm, B. Klinger, J. Alvarez, and K. D. v. Ellenrieder, "Controller Design Challenges for Waterjet Propelled Unmanned Surface Vehicles with Uncertain Drag and Mass Properties," 2013.

[8] J. Canny, "A computational approach to edge detection," *Pattern Analysis and Machine Intelligence, IEEE Transactions on,* pp. 679-698, 1986.

[9] opencv dev team. (2014). *OpenCV*. Available: http://opencv.org/

[10] L. Paull, S. Saeedi, M. Seto, and H. Li, "AUV Navigation and Localization: A Review," 2014.

[11] RFDesign Pty Ltd. (2013). *RFD900 Radio Modem Data Sheet*. Available: http://rfdesign.com.au/downloads/RFD900%20DataSheet.pdf

[12] qgroundcontrol. (2014). *MAVLink Micro Air Vehicle Communication Protocol*. Available: http://qgroundcontrol.org/mavlink/start

[13] Infocomm Development Authority of Singapore. (2014). *Spectrum Management Handbook*. Available: https://www.ida.gov.sg/~/media/Files/PCDG/Licensees/SpectrumMgmt/SpectrumNumMgmt/SpectrumMgmtHB.pdf

[14] Open Source Robotics Foundation. (2014). *actionlib*. Available: http://wiki.ros.org/actionlib

[15] N. Koenig, "Design and use paradigms for gazebo, an open-source multi-robot simulator

2004 IEEE/RSJ International Conference on Intelligent Robots and Systems (IROS) (IEEE Cat. No.04CH37566)," vol. 3, p. 2149, 2004.